Remote Sensing of Environment 127 (2012) 181–193

Contents lists available at SciVerse ScienceDirect

Remote Sensing of Environment

journal homepage: www.elsevier.com/locate/rse

Evaluation of potential of multiple endmember spectral mixture analysis (MESMA) for surface coal mining affected area mapping in different world forest ecosystems

Alfonso Fernández-Manso [a], Carmen Quintano [b,*], Dar Roberts [c]

[a] Agrarian Science and Engineering Department, University of León, 24400-Ponferrada, Spain
[b] Electronic Technology Department, University of Valladolid, 47014-Valladolid, Spain
[c] Department of Geography, University of California, Santa Barbara, CA 93106, United States

ARTICLE INFO

Article history:
Received 17 February 2012
Received in revised form 17 August 2012
Accepted 19 August 2012
Available online 28 September 2012

Keywords:
MESMA
SMA
Surface coal mining
Landsat

ABSTRACT

Surface coal mining (SCM) has undergone dramatic changes in the last 30 years. Large-scale SCM practices are at the center of an environmental and legal controversy that has spawned lawsuits and major environmental investigations. SCM techniques extract multiple coal seams by removing an area of many square kilometers and creating serious environmental problems. Information about mining activities location is essential for environmental applications, specifically the temporal and spatial patterns of land cover/land use change (LCLUC). Advancements in satellite imagery analysis provide possibilities to investigate new approaches for LCLUC detection caused by SCM globally. However there is no study that analyzes the changes produced for SCM at a global scale. Our work examines three areas of coal extraction in the world: Spain, United States of America (USA), and Australia. We used Multiple Endmember Spectral Mixture Analysis (MESMA) applied to Landsat Thematic Mapper (TM) data to map SCM affected area. Endmember spectra of vegetation, soil, and impervious surfaces were collected from the Landsat TM image with the help of a fine resolution orthophotographs and the pixel purity index (PPI). Reference endmembers from an Airborne Visible-Infrared Imaging Spectrometer (AVIRIS) spectral library were utilized as well. An unsupervised classifier was applied to the fraction images to obtain an estimation of active SCM affected area. Classification accuracy was reported using error matrixes and κ statistic using active SCM affected area perimeters digitized from fine resolution orthophotographs as reference data. In addition, we compared the accuracy of the MESMA based estimation to estimates using Spectral Mixture Analysis (SMA), and a spectral index traditionally used as Normalized Difference Vegetation Index (NDVI) testing statistical significance using a *Z*-test of their κ statistics. Results showed a significant improvement in the accuracy of the SCM affected area using MESMA with an average increase of the κ statistic of 31%. We conclude that MESMA-based approach is effective in mapping SCM active affected area.

1. Introduction

Mining, in general, and surface mining in particular may lead to severe environmental degradation. From an environmental point of view, surface coal mining (SCM) is a transforming activity with a high number of detrimental consequences, namely soil erosion, acid-mine drainage and increased sediment load as a result of abandoned and un-reclaimed mined lands (Parks et al., 1987). Over 6185 million tonnes (Mt) of hard coal is currently produced worldwide and 1042 Mt of brown coal/lignite. The largest coal producing countries are not confined to one region — the top five hard coal producers are China, the United States of America (USA), India, Australia and South Africa (World Coal Association, 2005). For example, surface mining accounts for around 80% of production in Australia; while in the USA it accounts for about 67% of production (International Energy Agency, 2011). These data indicate the importance of surface mining in the global production of coal.

SCM activity has important social, economic, political and environmental impacts on both local and global scale. At local scale many studies (e.g. García-Criado et al., 1999; Kennedy et al., 2003; Pond et al., 2008) have shown that coal mining activities negatively affect stream biota in nearly all parts of the globe. For example, Bernhardt and Palmer (2011) and Palmer et al. (2010) showed that the aquatic ecosystems of the Central Appalachians (USA) suffered water-quality degradation associated with acidic coal mine drainage as the sediments resulting from SCM (specifically mountain top removal), and chemical pollutants transmitted downstream through the river networks of the region. Similarly, Connor et al. (2004) showed a marked loss of biodiversity and water quality, as well as increased erosion, salinity, and siltation rates in large sections of the

* Corresponding author at: Electronic Technology Department, University of Valladolid, Industrial Engineering School (EII), C/ Francisco Mendizábal, s/n, 47014-Valladolid, Spain. Tel.: +34 983 186487; fax: +34 983 423490.
E-mail addresses: alfonso.manso@unileon.es (A. Fernández-Manso), menchu@tele.uva.es (C. Quintano), dar@geog.ucsb.edu (D. Roberts).

0034-4257/$ – see front matter © 2012 Elsevier Inc. All rights reserved.
http://dx.doi.org/10.1016/j.rse.2012.08.028

Upper Hunter Valley (New South Wales, Australia). At the global scale, the cumulative effect of significantly increasing coal extraction has serious implications for global warming and climate change, regarded as the most challenging environmental issue confronting the global community in the twenty first century. Methane, an important greenhouse gas contributing to global warming (Wuebbles & Hayhoe, 2002), appears naturally during the coal extraction process. In addition, generation of electricity and heat is the largest producer of CO_2 emissions, being responsible for 41% of the world CO_2 emissions in 2009 (International Energy Agency, 2011; United States Energy Information Administration, 2011). Worldwide, this sector relies heavily on coal, the most carbon-intensive of fossil fuels, amplifying its share in global emissions. Coal is widely used as a natural fuel and provides more than half the electricity consumed in USA. Countries such as Australia, China, India, Poland and South Africa produce between 68% and 94% of their electricity and heat through the combustion of coal (International Energy Agency, 2011).

Quantification of the effects that mining activities have on ecosystems is a major issue in sustainable development and resources management (Latifovic et al., 2005). Generating an environmental database for carrying out environmental SCM impact assessment is a difficult task by conventional methods. Due to its synoptic coverage and repetitive data acquisition capabilities, remote sensing has become an effective alternative to conventional methods for monitoring SCM. Compared to other environmental land cover changes studies, such as forest fires, fewer studies (e.g. Lévesque & Staenz, 2008; Rathore & Wright, 1993; Schmidt & Glaesser, 1998; Schroeter, 2011) have evaluated the potential of remote sensing for monitoring environmental impacts in mining areas. Moreover, fewer studies have examined the use of remote sensing to map surface mines. An exception is the review by Slonecker and Benger (2002) regarding remote sensing research on surface mining. Another is a summary by Erener (2011) who provides a comprehensive list of remote sensing applications, including utility in: mapping surface mine extent through time (Prakash & Gupta, 1998; Townsend et al., 2009; Wen-bo et al., 2008); detecting and monitoring coal fires (Mansor et al., 1994; Martha et al., 2010; Voigt et al., 2004); monitoring environmental impacts of SCM (Charou et al., 2010; Haruna & Salomon, 2011; Schmidt & Glaesser, 1998); discriminating mined areas and mapping industrial open pit mines (Fernández-Manso et al., 2005; Nuray et al., 2011; Richter et al., 2008; Wright & Stow, 1999) and mapping of mine reclamation (Erener, 2011; Straker et al., 2004; Townsend et al., 2009).

Most of these studies were based on the use of Landsat Thematic Mapper (TM) data (e.g. Schmidt & Glaesser, 1998; Toren & Ünal, 2001; Townsend et al., 2009), although other data have been used. For example, Charou et al. (2010) based their study on Advanced Spaceborne Thermal Emission and Reflection (ASTER) data; Mars and Crowley (2003) mapped mines wastes using the Airborne Visible-Infrared Imaging Spectrometer (AVIRIS) imagery; and Ellis and Scott (2004) used Hymap data. Original bands and vegetation indexes have been widely used (Latifovic et al., 2005; Martha et al., 2010; Prakash & Gupta, 1998; Shank, 2008; Wen-bo et al., 2008). There are, however, some studies based on different techniques. Townsend et al. (2009) studied the changes in the extent of surface mining and reclamation in the Central Appalachians using Support Vector Machine (SVM); and Charou et al. (2010) assessed the impact of mining activities by using Artificial Neural Networks (ANN) to classify remotely sensed data. Spectral Mixture Analysis (SMA) was employed by several authors including Fernández-Manso et al. (2005), who mapped forest cover changes caused by mining activities, Lévesque and Staenz (2008) who monitored mine tailings re-vegetation using multitemporal hyperspectral image, Richter et al. (2008) who quantified the rehabilitation process in mine tailing areas and Shang et al. (2009) characterized mine tailings.

Simple SMA provides an estimate of the proportions of different basic land cover types within a mixed pixel by using a fixed suite of endmembers for the decomposition of all pixels. However, within class spectral variability, and pixel-to-pixel variability in the number of endmembers required to unmix a pixel can cause large errors in the estimated fractional cover using simple SMA. Multiple endmember SMA (MESMA) (Roberts et al., 1998) decomposes each pixel using different combinations of possible endmembers, allowing a large number of endmembers to be utilized across a scene and of the number of endmembers to vary between pixels. For a given mixed pixel, too many endmembers may overfit the data yielding an unstable solution, while too few endmembers results in large residuals with the fraction of an unmodeled component partitioned into the fraction estimate of the selected endmembers (Li et al., 2005). MESMA assumes that although an image contains a large number of spectrally distinct components, individual pixels contain a limited subset of these.

Given the advantages of MESMA over SMA, our study aims to use MESMA to map SCM affected area (SCMAA) using Landsat. We define SCMAA as the active mining area plus non-reclaimed areas. Reclaimed areas are not included in this definition of 'affected area'. We compare the accuracy of the SCMAA estimation obtained using MESMA to the accuracy of SCMAA estimation based on more traditional methods including simple SMA and spectral indexes. Statistical significance is evaluated by means of *Z*-test of their κ statistics. We are unaware of any study that has used MESMA to analyze SCMAA. The most similar study is by Bedini et al. (2009) who applied MESMA to Hymap imaging spectrometer data to map mineralogy in the Rodalquilar caldera (Spain). Moreover, our work has the potential to be applied to different world forest ecosystems. We consider three study areas located in three countries, the USA, Australia and Spain. Again, we could not find any study about SCMAA mapping in three different continents, so we believe that our study is the first study of this type. Specifically, the objectives of the study are: 1) to evaluate the potential of MESMA in the discriminating of mining activities using Landsat TM images; and 2) to map accurately the areas affected by SCM exploitations.

2. Materials and methods

2.1. Study areas

We performed a full analysis of the main SCM areas globally before selecting our study areas. The analysis was based on the InfoMine international data base (www.infomine.com) where mining activity is collected worldwide. The criteria used to select the study areas were to choose areas where SCM affected areas had high environmental value (mainly forests) and where environmental impacts have been greater. Additionally, we took into account the availability of cloud-free Landsat-5 TM images. We considered initially six potential study areas: El Bierzo (Castilla y León — Spain), Eastern Kentucky (USA), Upper Hunter Valley (New South Wales — Australia), Jharia (India), Seyitömer (Turkey), and Witbank (South Africa), though only the first three areas were ultimately selected: (Fig. 1, Table 1).

El Bierzo county (Spain) is in a sheltered mountain valley on the Northwestern boundary of the province of León, in the autonomous region of Castilla y León (Spain), and defined by longitude −6.64 E and latitude 42.99 N. Elevation ranges between 660 and 1900 m. Mean annual rainfall is 1500 mm and temperatures range from a summer high of 32 °C to a winter low of 1 °C with a year-round average of 10 °C (AEMET, 2011). El Bierzo has 6 mines currently in operation (3 open cut; 3 underground), and produced a total of 5 Mt of raw coal (anthracite) in 2009 (Spanish Ministry of Industry, Tourism and Business, 2009). The main vegetation cover is Atlantic oak forest (*Quercus* sp.) and scrub (*Erica* sp.).

The second study area, the Eastern Kentucky Coalfield Region, covers 31 counties with a combined land area of 35 km. It is part of

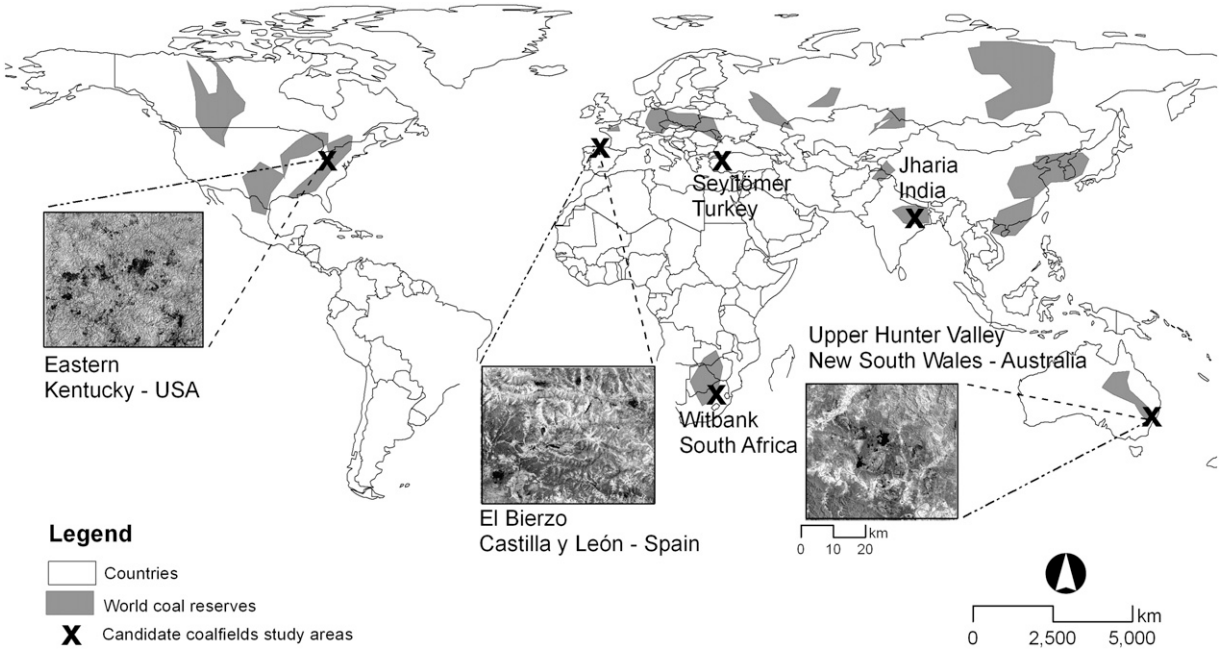

Fig. 1. Study areas location.

a larger physiographic region called the Cumberland Plateau. This escarpment is formed from resistant Pennsylvanian-age sandstones and conglomerates. The area is dominated by forested hills and highly dissected by V-shaped valleys (350 m average elevation range). In general, the elevations of the hills are highest in southeastern Kentucky where the highest elevation, 1263 m (before mining), was at Black Mountain. The majority of the mature forests are populated by oaks (*Quercus* spp.) including both white and red oaks. However, yellow-poplar (*Liriodendron tulipifera*), is also an extremely important timber species. Other important species are hard maple (*Acer saccharum* and *Acer nigrum*) and ash (*Fraxinus* spp.). Bituminous coal deposits in the eastern coal field are lower in sulfur content, averaging between 1 and 2 percent by weight. By 2010, 44.2 Mt of coal were extracted from Kentucky Eastern Coalfield (Department for Energy Development and Independence, 2010).

Our third study area, the Upper Hunter Valley region, is situated in rural New South Wales (NSW), in southeastern Australia, approximately 200 km northeast of Sydney. Over the last three decades, coal mining, energy production and associated businesses have become major industries in this region. The Upper Hunter has 19 mines currently in operation (12 open cut; 4 underground; 3 both open cut and underground), and produced a total of 106.87 Mt of raw coal in 2008. This represents around two thirds of total coal production for NSW and 40% of total Australian black coal production (Minerals Council of Australia, 2010). The valley has a variable climate depending on elevation and proximity to the coast. Coastal areas and the area around the Barrington Tops receive the highest rainfall of around 1140 mm per year, with rainfall decreasing with distance inland. Rainfall at Muswellbrook averages 640 mm per year, with December and January the wettest months. The climate of the upper Hunter catchment is characterized by hot summers, averaging about 30 °C in January, with periods of humid, stormy conditions; winters are cool to mild and dry. Temperature extremes tend to be highest in the west of the catchment. Dry Sclerophyll forests are the main vegetation cover. This forest is a woodland of 15–20 m tall (*Eucalyptus* sp.), mixed with an open to sparse sclerophyll shrub stratum (*Acacia* sp.) and open groundcover of tussock grasses (Thomas et al., 2000).

2.2. Remotely sensed data

Three Landsat-5 TM scenes downloaded from US Geological Survey (USGS) (www.glovis.usgs.gov) were used. All of the images had an L1G level of processing (systematic correction), which implies that the data product provides systematic radiometric and geometric accuracy, and that the scene is rotated, aligned, and geo-referenced to the UTM map projection. Table 2 shows the main characteristics of each scene.

2.3. Ancillary geospatial data

Several ancillary data were used in the different stages of the methodology. The ASTER Global Digital Elevation Model Version 2 (GDEM V2), provided by USGS, was employed to perform topographic normalization of the Landsat TM images. Fine resolution

Table 1
Summary of the main characteristics of potential study areas (*: definitively selected study areas).

Country	State	Region	Elevation (average) (m)	Forest Ecosystem	AAR (mm)	AAT (°C)	Coal type	ACP (Mt)
* Spain	Castilla y León	El Bierzo,	660–1900 (1300)	Atlantic oak forests	1500	10	Anthracite	5.0
* USA	Kentucky	Eastern Kentucky	250–1300 (350)	Mixed mesophytic Appalachian aak	1200	13	Bituminous	44.2
* Australia	New South Wales	Upper Hunter Valley	20–625 (250)	Dry sclerophyll forests	900	16	Lignite	106.9
India	Jharkhand	Jharia Dhanbad	100–400 (225)	Subtropical dry sessional forest	1300	23	Bituminous	85.0
Turkey	Kütahya	Seyitömer	1000–1300 (1100)	Temperate forests	500	13	Lignite	7.0
South Africa	Mpumalanga	Witbank	300–800 (500)	Subtropical grasslands and sabannas	610	18	Bituminous	174.0

Note: AAR: Annual average rainfall; AAT: Annual average temperature; ACP: Annual coal production.

orthophotographs were used to validate the SCMAA estimations. Specifically, we used 50 cm orthophotographs, acquired during midsummer 2010 provided by the Spanish National Center of Geographic Information (CNIG; http://www.cnig.es/) through the Spanish Aerial Ortho-photography National Planning (PNOA) in the Spanish study area. For the Kentucky study area, we used 1 m true color orthophotographs, acquired during 2007 midsummer, and provided by the National Agriculture Imagery Program (NAIP). Finally, 1 m spatial resolution orthophotographs acquired during 2010 summer were used in the Australian study area, provided by the New South Wales Natural Resource Atlas (http://www.nratlas.nsw.gov.au/).

Additionally, a 2007 3.5 m spatial resolution AVIRIS image of the University of California, Santa Barbara, was used as a source of impervious and soil spectra. All AVIRIS spectra were extracted from reflectance images atmospherically corrected using Modtran radiative transfer code and a ground reference target (see Herold et al., 2004; Roberts et al., 2012).

2.4. Methods

The methodology involved three parallel image analysis techniques: MESMA, SMA and vegetation indexes (Fig. 2). Prior to image analysis, the Landsat-5 TM images were pre-processed, including image subsetting, topographic normalization and atmospheric correction. After the creation of a spectral library, we applied the SMA and MESMA algorithms to obtain the image fractions. Both the images fractions and the vegetation indices were classified using ISODATA to estimate the SCMAA. Accuracy of all SCMAA estimations was computed using an error matrix and κ statistic. A *Z*-test allowed us to evaluate whether accuracy difference were statistically significant between approaches.

2.4.1. Pre-processing

First of all, the scenes were subset to the selected study areas. Table 2 shows the size (average size equals aprox. 1700 km^2) and latitude/longitude coordinates of each subset. The subset images were co-registered to the orthophotographs using nearest-neighbor resampling, resulting in a mis-registration error between the TM images and orthophotographs below one quarter of a TM pixel. After the co-registration, the images were topographically normalized using the C-correction algorithm developed by Teillet et al. (1982) with the help of the GDEM V2 and knowledge of the solar zenith and azimuth angle at the moment of image acquisition. Finally, the Landsat TM images were converted to apparent surface reflectance. The original digital numbers of reflective TM bands were scaled to radiance values (L_λ) using the procedure proposed by Chander and Markham (2003). The radiance to surface reflectance (ρ) conversion was performed by using the image-based cosine of the solar transmittance (COST) method (Chavez, 1996). Path radiance (L_p) values were computed by using the formulae reported in Song et al. (2001), which assumes 1% surface reflectance for dark objects (Chavez, 1989, 1996). The optical thickness for Rayleigh scattering (ρ_r) was estimated according to the equation given in Kaufman (1989).

Digitizing of surface mines at large scales is a very effective method for accurately documenting surface mining activity. Following this idea, the perimeters of SCM affected areas were digitized using high-resolution orthophotographs to act as ground reference data to assess the accuracy of the different SCMAA estimates (Fig. 3).

Under the 'unmixing' caption of Fig. 2, we included three key processes: spectral library creation; SMA and MESMA. Fig. 4 shows a detailed flowchart of this stage of the methodology. Though from a chronological point of view we built the spectral library before applying SMA/MESMA, we described the SMA/MESMA processes before the creation of the spectral library for a better understanding.

2.4.2. SMA/MESMA algorithms

SMA is generally defined as the calculation of land cover fractions within a pixel (Roberts et al., 1998). Unmixing considers that each pixel can be represented as a weighted linear combination of the selected endmembers, with the weight being the endmember fractions, and a residual (Eq. 1).

$$x = Mf + e \quad (1)$$

where x is the n-dimension reflectance vector; n, the number of bands used; c, the number of endmembers used; M, n×c, the endmember spectra matrix; f, c-dimensional fraction vector; and *e*, n-dimensional error vector, representing the residual error.

The aim of spectral unmixing is to solve Eq. (1) for each pixel of the image, obtaining f, with x and M knowns. In this way, a fraction image is obtained for each endmember considered, which represents the percentage of that endmember in the original data. If the number of endmembers defined together with their spectral signatures have been correctly characterized, f will conform to the following conditions: (1) all its elements are greater than or equal to zero and less than or equal to one; (2) the sum of all of them is unity; and (3) the error term, *e*, will be negligible (Quintano et al., 2006). There are different methods for solving Eq. (1). Singular value decomposition is one of them, and it is the methods used by the software package used in this work, VIPER Tools (Roberts et al., 2007).

MESMA is an extension of SMA that addresses spectral and spatial variability within material classes by allowing the number and type of endmembers to vary on a per pixel basis (Roberts et al., 1998). Rather than using waveband selection or spectral transformation techniques to reduce endmember variability, MESMA enables the user to select multiple endmembers to represent each material class. By using VIPER Tools open-software (Roberts et al., 2007), MESMA unmixing can be accomplished with two, three or four endmembers, which is comprised of one, two or three classes endmember coupled with a shade endmember (Dennison et al., 2007; Roberts et al., 1998). The chosen model for each pixel, i, is the one that minimizes the root

Table 2
Dataset characteristics.

Study area	Image						Windowed image (analyzed area)	
	Sensor	Source	Path	Row	Date	Projection/datum	Area (km^2)	Lat–Lon (center of windowed image)
Spain	Landsat-5 TM	USGS	203	30	24 June 2011	UTM-30N /WGS-84	1788.31	−6.6462 E 42.9907 N
USA	Landsat-5 TM	USGS	19	34	3 June 2006	UTM-17N /WGS-84	1464.63	−83.4090 E 37.5358 N
Australia	Landsat-5 TM	USGS	90	82	20 October 2011	UTM-56S /WGS-84	1974.71	150.7248 E 32.2070 S

Note: TM, Thematic Mapper; USGS, US Geological Survey; UTM, Universal Transverse Mercator; WGS, World Geodetic System.

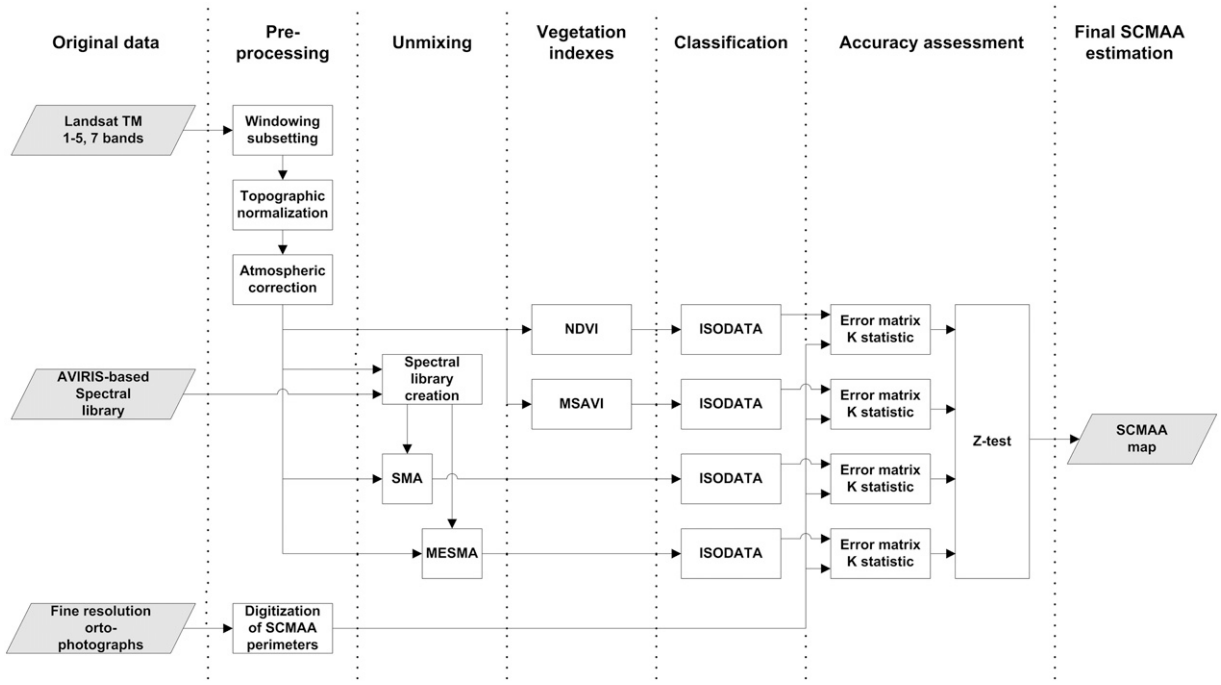

Fig. 2. Methodology flowchart.

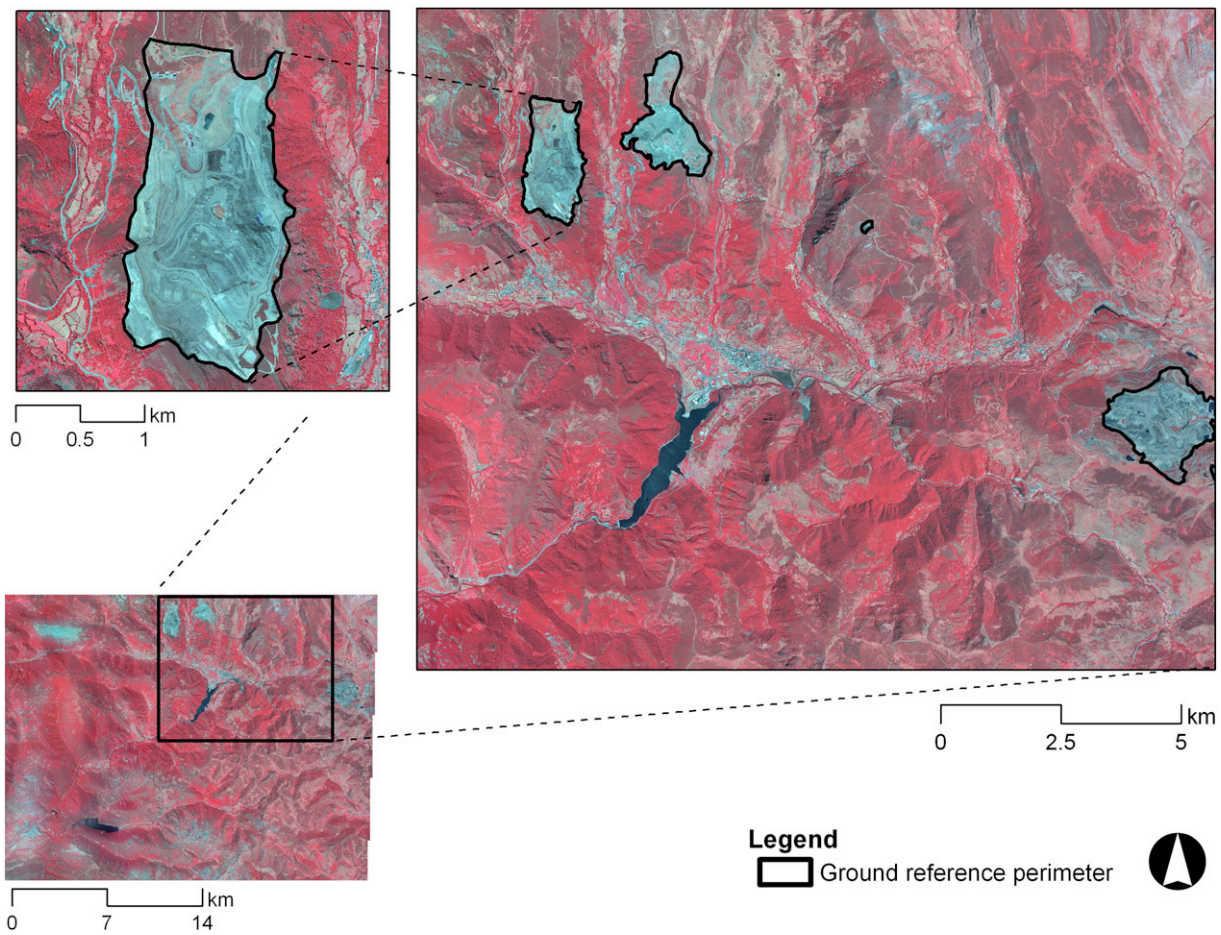

Fig. 3. Reference surface coal mining affected area (SCMAA) perimeter digitized using a 50 cm orthophotograph (Spanish study area).

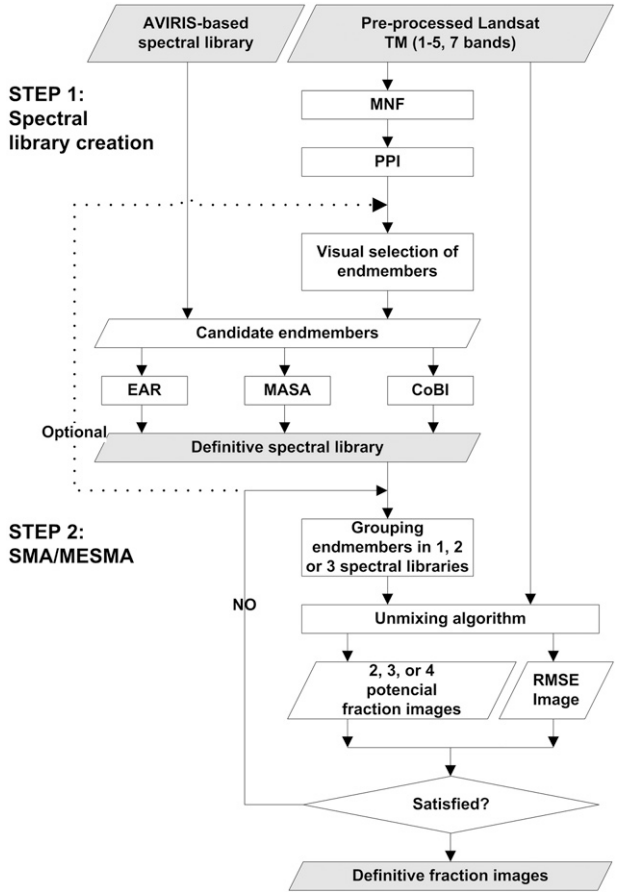

Fig. 4. Detailed flowchart of the 'unmixing' step of the proposed methodology.

mean square error (RMSE) over the included number of bands, B, used in unmixing (Eq. 2):

$$RMSE_i = \left[\sum_{k+1}^{B}\left(\varepsilon_{i,k}\right)^2/B\right]^{1/2} \quad (2)$$

The VIPER Tools software used in our study allowed us to fix the minimum and maximum allowable fraction values, the maximum allowable shade fraction value, and the maximum allowable RMSE to obtain the fraction images by applying MESMA to the original Landsat-5 TM images. Specifically, the following values were employed in our study: minimum and maximum allowable fraction values, −0.05 and 1.05, respectively; maximum allowable shade fraction value, 0.8; and maximum allowable RMSE, 0.025.

2.4.3. Spectral library creation

Before applying SMA/MESMA we needed to define the endmembers to unmix the Landsat images. Endmember selection is the most important step in SMA/MESMA. It determines how accurately the mixture models can represent the spectra (Tompkins et al., 1997). The endmember selection must accommodate the dimensionality of the mixing space. It involves determination of the number of endmembers and the methods to select these endmembers. The definition of appropriate spectral endmembers may be either done using reference endmembers from spectral libraries or from the image itself (image endmembers). We formed our spectral library from two sources: the Landsat images (image endmembers) and an AVIRIS-based spectral library (reference endmembers). As image endmembers we mainly included vegetation and mining surfaces, whereas reference endmembers were mostly impervious surfaces and soil spectra.

To select the image endmembers, we first applied a minimum noise fraction (MNF) transformation and the pixel purity index (PPI) algorithm (Boardman et al., 1995). MNF (essentially two cascaded principal components transformations) was used to determine the inherent dimensionality of image data, to segregate noise in the data, and to reduce the computational requirements for subsequent processing (Boardman & Kruse, 1994). The data space could then be divided into two parts: one part associated with large eigenvalues and coherent eigenimages, and a complementary part with near-unity eigenvalues and noise dominated images. By using only the coherent portions, the noise was separated from the data, thus improving spectral processing results. The new MNF transformed bands were then analyzed to find the most spectrally pure (extreme) pixels in the image using PPI. The PPI image was the result of several thousand iterations of the PPI algorithm. The higher values indicated pixels that are relatively purer than pixels with lower values (Environment for Visualizing Images, ENVI, 2009). Once the purest pixels were located, we selected a subset identifying each endmember type based on their spectra and local knowledge. From the AVIRIS-based spectral library we selected reference endmembers for surfaces that could not be readily identified in the Landsat-5 TM images. Specifically, we used mainly endmembers that characterized impervious surfaces as roads and roofs. Due to the limited spatial resolution of Landsat-5 TM images, it was difficult to find pure pixels that represented impervious surfaces. The endmembers of the AVIRIS-based spectral library helped us to solve this limitation.

Once the spectral library with the candidate image and reference endmembers was created three indices for identifying optimal endmembers were used: Endmember Average RMSE (EAR); Minimum Average Spectral Angle (MASA); and Count-based Endmember Selection Index (CoBI). All of them are included in the VIPER Tools open-software package (Roberts et al., 2007) that was used to implement the MESMA algorithm. Endmember selection is an important aspect that should take into consideration the spectral diversity of the library and computational efficiency, since a spectral library can be comprised of hundreds of spectra for each material class (Dennison & Roberts, 2003a; Dennison et al., 2004). By using these indexes, we selected the optimal endmembers and created the definitive spectral library to unmix the Landsat-5 TM images.

EAR (Eq. (3)) selects the endmembers that produce the lowest root mean squared error (RMSE) within a class (Dennison & Roberts, 2003b).

$$\mathrm{EAR}_i = \sum_{j=1}^{N}\mathrm{RMSE}_{i,j}/(n-1) \quad (3)$$

where i is an endmember, j is the modeled spectrum, N is the number of endmembers, and n is the number of modeled spectra. The "−1" corrects for the zero error resulting from an endmember modeling itself.

MASA chooses the endmembers that produce the lowest average spectral angle (Dennison et al., 2004). MASA is similar to EAR, but uses a spectral angle (θ) as the error metric. Spectral angle is calculated as shown in Eq. (4).

$$\theta = \cos^{-1}\left(\sum_{\lambda=1}^{M}\rho_\lambda\rho'_\lambda/L_\rho L_{\rho'}\right) \quad (4)$$

where $\rho\lambda$ is the reflectance of a endmember, $\rho'\lambda$ is the reflectance of a modeled spectrum, $L\rho$ is the length of the endmember vector and $L\rho'$ is the length of the modeled spectrum vector calculated as displayed in Eq. (5). MASA is then calculated as shown in Eq. (6):

$$L_{\rho'} = \sqrt{\sum_{k=1}^{M}\rho_k^2} \quad (5)$$

$$MASA_i = \sum_{j=1}^{N} \theta_{i,j}/(n-1) \quad (6)$$

Finally, CoBI selects endmembers that model the greatest number of spectra within their class (Roberts et al., 2003). It can be used to rank endmember selection based on maximizing the models selected within the correct class, while minimizing confusion with other classes. CoBI uses the MESMA concept to select endmembers based on the number of library spectra each endmember models. CoBI determines the number of spectra modeled by an endmember within the endmember's class (InCoB) and outside of the endmember's class (OutCoB). The optimum model would have the highest InCoB and lowest OutCoB.

As shown in Fig. 4, our proposed methodology is iterative; we unmixed the image varying the types of materials included in each class (e.g., soil and NPV), the number of spectra within each class and the complexity of the models (i.e., two, three or four endmember models) until the fraction images obtained produced an accurate SCMAA estimation. In some cases, when the percentage of classified pixels was too low, the spectral library needed to be refined by introducing a new type of spectrum to model the unclassified areas.

The iterative procedure we used can be summarized as follows. Starting with a two-endmember model (one class and shade), we unmix the image by grouping in a class: 1) GV and coal mines; 2) GV, bare soil and coal mines; and 3) GV, bare soil, water and coal mines. None of these two-endmember models allowed us to obtain fraction images that produced an accurate SCMAA estimation. In some cases, the percentage of classified pixels was too low; and in others cases, the SCMAA estimate accuracy was unacceptable. Considering three-endmember models (two classes and shade), we varied the type of material included in each class. After several trials, we observed that using biotic class (GV-NPV) and abiotic class (SCM-Soil) produced simultaneously an accurate SCMAA estimate and a low number of unclassified pixels. Besides these facts, the hierarchical scheme that we followed (see Table 3) could be used with small variations (only at level 3) in the three study areas so we could propose a general method that works in different world forest ecosystems. We tried four-endmember models as well to check if the SCMAA estimate accuracy could be increased. The increase in accuracy, however, was too low compared to the increase in complexity to group the materials into three classes; so we decided to follow the scheme of Table 3 in all three study areas.

Specifically, endmembers were selected based on a hierarchical classification scheme with three levels, Impervious-pervious (Level 1), endmember class (i.e., GV, NPV, etc.; Level 2) and endmember type (i.e., forest, open forest, scrub, etc.; Level 3). A key goal then was to identify optimal endmember sets that captured the spectral diversity of the biotic components (GV-NPV) and abiotic components (SCM-Soil) and produced accurate, stable fractions of mine affected area.

2.4.4. Vegetation indices

For the three Landsat-5 TM images, we calculated Normalized Difference Vegetation Index (NDVI) (Rouse et al., 1973) and Modified Soil-Adjusted Vegetation Index (MSAVI) images (Qi et al., 1994a, 1994b), hypothesizing that these two indices would increase the separability of mined and reclaimed areas from other cover types. The NDVI has been frequently used in surface mining studies and has proven useful to map the areas affected by this activity (Erener, 2011; Prakash & Gupta, 1998). MSAVI, and its later revision MSAVI2 (Eq. 11), are soil adjusted vegetation indices that seek to address some of the limitation of NDVI when applied to areas with a high degree of exposed soil surface. Qi et al. (1994a) developed the MSAVI, and later the MSAVI2 (Qi et al., 1994b) to more reliably and simply calculate a soil brightness correction factor. MSAVI2, though often called MSAVI, has been used in a number of erosion studies, where bare soil is one of the most important covers (Liu & Wang, 2005). As is true for most studies, we used the MSAVI2 version of the index, though we refer it as MSAVI.

$$MSAVI2 = \left(2NIR + 1 - \sqrt{(2NIR + 1)^2 - 8(NIR - RED)}\right)/2 \quad (7)$$

where RED and NIR are respectively the red and near-infrared reflectance.

2.4.5. Classification

The ISODATA clustering algorithm was used to classify the SMA and MESMA fraction images as well as NDVI and MSAVI images. ISODATA is one of the most commonly used of the remote sensing unsupervised classification algorithms (Jensen, 1996). We used 10 classes in all cases so the influence of the classifier in the final accuracy of SCMAA estimations was minimized. A 3×3 median filter was applied as post-classification procedure.

Table 3
Endmember signatures included in the definitive spectral library hierarchically grouped.

Hierarchical levels			Spectral library	Origin	Endmembers per study area		
Level 1	Level 2	Level 3			Spain	USA	AU
Pervious	GV	Forest	GV&NPV	TM	1	2	1
		Open forest	GV&NPV	TM	1	1	1
		Scrub	GV&NPV	TM	1	1	
		Grass	GV&NPV	TM		2	
		irrigated crop	GV&NPV	TM			1
		Unirrigated crop	GV&NPV	TM	1		1
	NPV	NPV	GV&NPV	AVIRIS		1	
	Bare soil	Bare soil	SCM&SOIL	AVIRIS		1	
	Water	Rivers	SCM&SOIL	TM		1	
		Lakes/Basins	SCM&SOIL	TM	1	1	1
Impervious	Coal mines	Wall	SCM&SOIL	TM		1	1
		Coal seam	SCM&SOIL	TM	1	1	1
		Mud basin	SCM&SOIL	TM		1	
		Bare rock	SCM&SOIL	TM	1	1	1
	Road	Asphalt	SCM&SOIL	AVIRIS	1	1	1
	Urban	Roof	SCM&SOIL	AVIRIS	1	1	1
		Urban mixture	SCM&SOIL	TM	1	1	
				# Endmembers in GV&NPV	4	7	4
				# Endmembers in SCM&SOIL	6	10	6
				# Models used in unmixing	24	70	24
				Image classified (%)	92.3	99.26	98.6

Note: GV&NPV: green vegetation and non-photosynthetic vegetation; SCM&SOIL: surface coal mines and soil; AU: Australia.

2.4.6. Accuracy assessment

We validated the SCMAA estimations using error matrices and the κ statistic (Congalton & Green, 2009). The resulting κ statistic indicates whether the confusion matrices are significantly different from a random result. Other accuracy statistics were also considered: overall accuracy (OA), producer's accuracy (PA) (omission error) and user's accuracy (UA) (commission error). As ground reference we used the SCMAA digitized from the fine resolution orthophotographs. To check whether classification results were a significantly different between a pair of SCMAA estimates, we used a *Z*-test based on the κ statistics of both estimations. Note that $z_c = 1.96$ at the 95% confidence level, and that the null hypothesis H0: $(k1 - k2) = 0$ is rejected when $Z > z_c$. Previously to compute the error matrices, we applied a random sampling over the ground truth image (20% of SCMAA and 10% of the unaffected area were considered).

3. Results

As presented in Methods, we used both reference and image endmembers to construct our spectral library. As shown in Fig. 4, the candidate image endmembers were selected visually among the purest signatures, located after applying MNF transform and PPI to Landsat images. The selection strategy was to try to catch the variability of both classes of interest: SCM affected and unaffected area. Therefore, we looked for spectral signatures inside and outside the SCMAA perimeters with the intention of seeking the highest contrast and separability of both classes. Specifically, and as an example, we found four different types of spectra that represented the variability in the American SCMAA: wall, coal seam, mud basin, and bare rock. The candidate reference endmembers from the AVIRIS-based spectral library were added to the candidate image endmembers. The reference endmembers provided mainly information on anthropogenic areas, specifically in mixing surfaces (urban and degraded areas) where it was difficult to find pure spectra in the Landsat images. Finally, multiple criteria were used to choose the definitive endmembers to be included in the spectral library using EAR, MASA and CoB. We gave preference to endmembers whose EAR and MASA were lower and CoB was higher.

Table 3 displays the hierarchical grouping of the endmember signatures included in the definitive spectral library. We defined three levels searching for equivalence among the types of endmembers of the three study areas. The first level distinguished between pervious and impervious surfaces; the second level grouped GV, NPV, bare soil and water in to the pervious level, and coal mines, roads and urban surfaces in to the impervious one; finally, the third level detailed some classes of the level 2, allowing the variability among the different study areas. In our final models 10, 17 and 10 different endmembers were used, respectively, in the modeling of the Spanish, American and Australian study area. Due to greater complexity of land use in USA study area, where large reclaimed areas, extensive urban areas and a large road network were present, we needed a higher number of endmembers in this area. These endmembers were grouped in to two spectral libraries: green vegetation and non-photosynthetic vegetation (GV&NPV), and surface coal mines and soil (SCM&SOIL). Table 3 also shows the number of models used to unmix the images in each study area (24, 70 and 24, respectively). In all cases, three fraction images: SCM&SOIL, GV&NPV and shade were obtained.

Fig. 5 shows the spectral signatures of four of the most representative endmembers of the study: forest, scrub, coal mines and urban. It is remarkable that the fundamental pattern of these spectra was the same over all the study areas with the only difference in value. Despite the different types of coal mining surfaces that exist at global scale, all of them are mainly characterized by: wide surfaces devoid of vegetation, large road infrastructures, high walls, coal seams, large holes (100 m depth), water surfaces and charcoal stores. These altered surfaces contrast with the natural areas in which they are embedded. As intermediate land use, especially in USA, there are large surfaces where vegetation was restored. These reclaimed areas, especially in their early stages, are an important cause of confusion in differencing SCM affected and unaffected areas because the bare floor with an herbaceous cover can be easily confused with SCMAA.

As shown in Table 3, the percentage of pixels classified was over 90% in all study areas, rising to 98% and 99% in two of them. These figures and the visual evaluation of the fraction images showed that the modeling was generally good, accurately identifying many of the SCMAA. As an example, Fig. 6 displays the fraction images obtained in the Spanish study area. Both the SCM&SOIL and GV&NPV fraction images show an important contrast between SCMAA and background. It can be observed in the SCM&SOIL fraction image zoom that this fraction detects with great precision the areas affected by surface coal mining and that it would be even possible to identify the different levels of impact on the vegetation inside the SCMAA, what could serve to establish severity levels of surface mining in a future work.

UA, PA, OA and κ statistic of the different SCMAA estimations in each study area are provided in Table 4. The *Z*-test showed that all estimates were significantly different. The MESMA-based estimate was the most accurate in all three study areas (κ equaled 0.75, 0.85 and 0.89 respectively in Spain, USA and Australia). Moreover, this estimate showed a greater balance between UA and PA. In contrast, the NDVI-based estimate displayed an unequal performance in the different study areas. In the Spanish study area, it had a low *k* statistic. Its lower UA (high commission error) indicates that there was significant confusion between SCMAA and areas with bare soil and rocks. The main reason for this confusion is surface heterogeneity in the Spanish area, including old burned scars, scrub, and eroded areas, in addition to subsurface mines. On the other hand, the NDVI-based estimate in the American study area had the second highest accuracy. Regarding the SMA-based estimation, it displayed a high stability, showing a relatively high accuracy in all of the study areas. Finally, the least accurate estimates were based on MSAVI. This index did not perform as well as expected.

To complement the accuracy analysis displayed in Table 4, Table 5 shows the SCMAA estimated by each method classified by the unsupervised classifier as well as the SCMAA obtained from the ground reference image. MESMA-based estimates achieved results that were closest to the actual value. The imbalanced performance of the NDVI-based estimate as well as the underestimate of SCMAA using MSAVI can also be observed (Table 5). Finally, Fig. 7 shows the map of SCMAA estimated by each input considered in the Australian study area. The image shows graphically the results discussed in Tables 4 and 5.

4. Discussion

Hierarchical grouping of the endmember signatures included in the definitive spectral library allowed us to generate three fraction images: GV&NPV (biotic), SCM&SOIL (abiotic), and shade in our three study areas. Both the number and the type of fraction images coincide well with the number and type found previously by other authors. Fernández-Manso et al. (2005) used these three same types of fraction images (obtained by SMA) to map the forest surface affected by mining activities. Specifically, the authors found that mining affected areas (dark and light), vegetation (GV) and shade fraction images led to the most accurate estimate of forest areas affected by mining activities. Similarly, Adams and Gillespie (2006) found that the ability to discriminate components depends on the properties of each type of landscapes. In particular they stated that three endmembers: GV (green leaves in canopy and in understory), soil/rock, and shade, are the most adequate set to model landscapes similar to ours. In particular, our results illustrate the importance of building an abiotic spectral library, SCM&SOIL, which reflects the

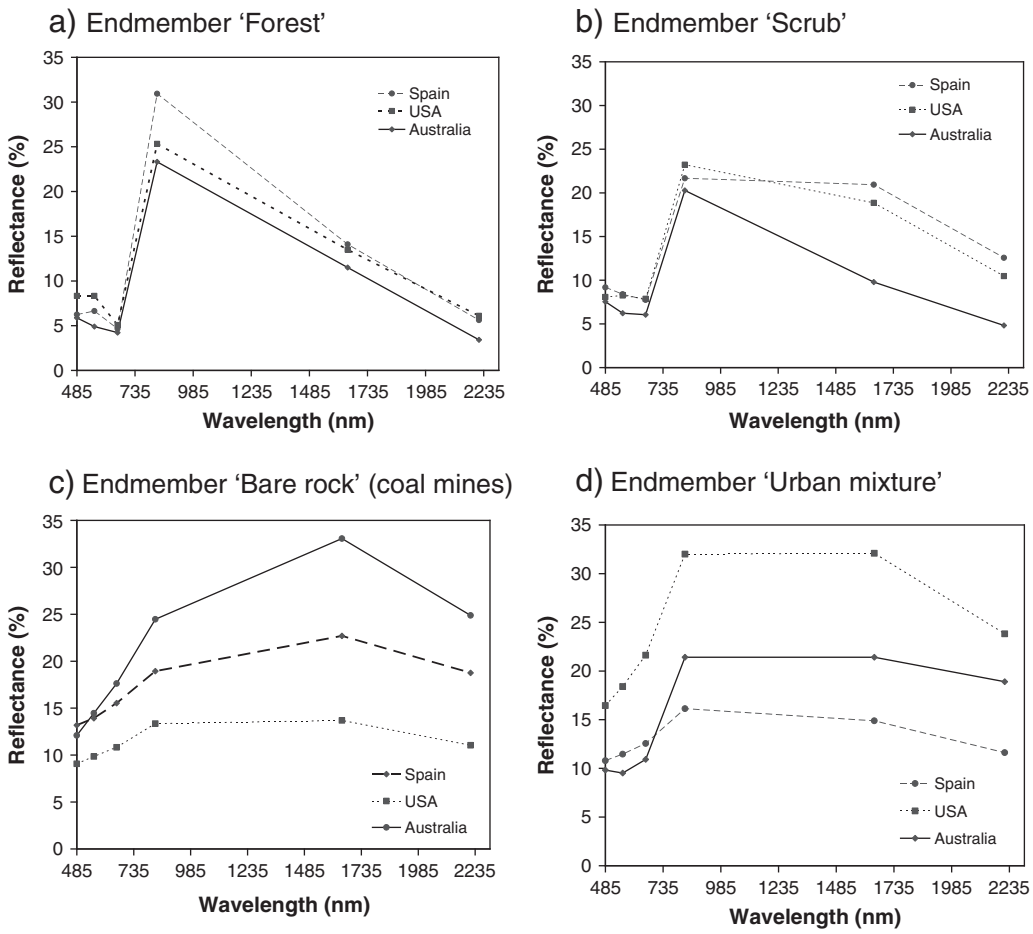

Fig. 5. Spectral signatures of some of the most representative endmembers.

land use impacts on the landscape as mining versus the green vegetation or forests. MESMA, by accounting for spectral heterogeneity, is better able to model spectrally variable human modified landscapes. We hypothesize that MESMA based SCMAA estimates had the highest accuracy in all three study areas because MESMA better accounted for this heterogeneity, especially in abiotic surfaces. Similar results have been found in urban areas (i.e. Lu & Weng, 2004; Rashed et al., 2003; Wu, 2004) where spectral heterogeneity is high.

Concerning the performance of MESMA versus SMA, we did not find any study that compared these two techniques. There are some studies, however, that used fraction images derived from SMA to identify mine affected areas. Lévesque and Staenz (2008) monitored mine tailings re-vegetation using multitemporal hyperspectral images. In their work, total vegetation fraction (high/low photosynthetic), total tailings fraction (fresh/oxidized), and texture of the vegetation fraction were used in a *K*-mean unsupervised classification, producing an OA equal to 78.13% and a κ statistic of 0.74. A similar value of κ statistic was obtained by Fernández-Manso et al. (2005), who developed a model involving segmentation of the shade fraction image into objects and classification based in membership functions to map mining affected areas in North Spain from Landsat data. OA in this study was estimated to be 84.91% and κ statistic was 72.05%. Richter et al. (2008) quantified the rehabilitation process in the Kam Kotia mine (Canada). Their study combined constrained SMA and threshold-based classification. With this procedure they retrieved fraction maps of major mine tailings-related surface materials and hence generated a surface map separating green vegetation, transition zones, dead vegetation, and oxidized tailings, and calculated the extent of each of the zones. The four zones were correlated with the extent and degree of vegetation cover affected by tailings material. Finally, Shang et al. (2009) characterized mine tailings in Northern Canada from fraction images obtained by applying SMA to hyperspectral remote sensing data. Unlikely, as many of other studies (as Erener, 2011; Latifovic et al., 2005; Prakash & Gupta, 1998; Martha et al., 2010; Shank, 2008; Wen-bo et al., 2008), they did not include a quantitative accuracy assessment.

Among the studies which evaluated accuracy, Townsend et al. (2009) calculated the PA and UA of mined and reclaimed cover classes in the Central Appalachians during 1999 to 2006 from NDVI Landsat images, specifically: PA varied from 66.7% to 77.8%, and UA, from 76.9% to 82.4%. Their results show the unequal performance of this vegetation index when the year of study varied. This conclusion agrees with our results showing dissimilar performance of NDVI over the different study areas. On the other hand, Schmidt and Glaesser (1998) monitored the environmental impacts of open cast lignite mining in Eastern Germany from Landsat images by using a maximum likelihood classifier. They were not able to calculate the classification accuracy for all the Landsat TM images because of the lack of reference data for all dates. To provide some measure of accuracy, they defined the percentage accuracy as the ratio of the number of hectares classified for a certain feature to the number of hectares for the same feature measured from the reference data (field data and aerial photographs). Using this metric, their average classification accuracy over the period 1989–1994 was 82.7% for the surface mine features and 86.1% for the reclaimed features. These figures, however, are difficult to compare to our accuracy results.

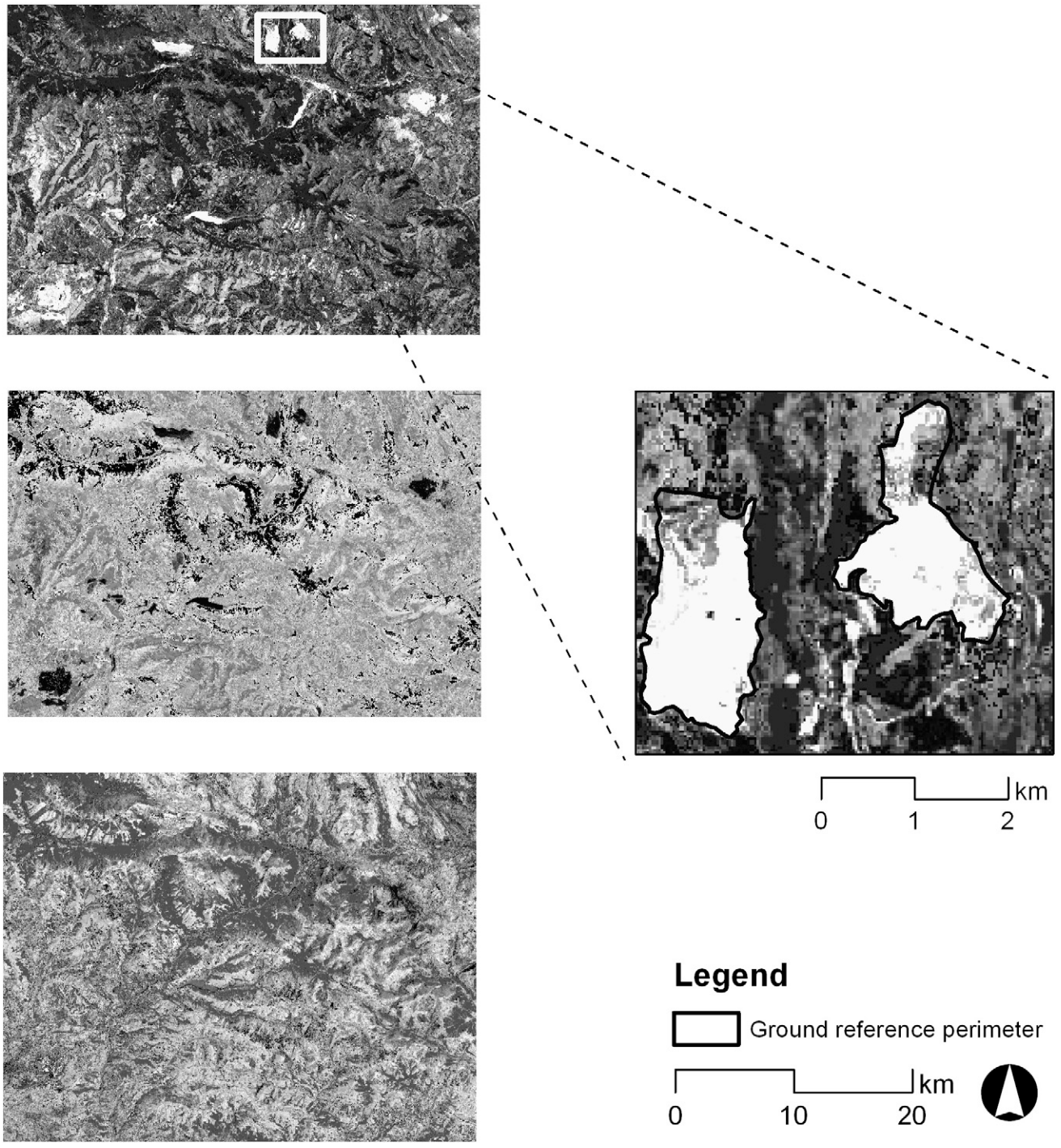

Fig. 6. MESMA-based fraction images in the Spanish study area. Upper left: SCM&SOIL fraction image; center left: GV&NPV fraction image; down left: shade fraction image, right: zoom of the SCM&SOIL fraction image.

Table 4
User's Accuracy (UA), Producer's Accuracy (PA), Overall Accuracy (OA), κ statistic and standard deviation of κ statistic (σ_κ) of the Surface Coal Mining Affected Area (SCMAA) estimations.

Image classified	Spain					USA					Australia				
	UA	PA	OA	κ	σ_κ	UA	PA	OA	κ	σ_κ	UA	PA	OA	κ	σ_κ
NDVI	0.57	0.87	0.81	0.20	0.0023	0.82	0.93	0.94	0.73	0.0026	0.90	0.94	0.96	0.84	0.0015
MSAVI	0.62	0.93	0.91	0.36	0.0034	0.95	0.76	0.95	0.65	0.0034	0.95	0.70	0.91	0.52	0.0027
SMA	0.81	0.83	0.98	0.64	0.0049	0.79	0.92	0.93	0.67	0.0027	0.91	0.94	0.96	0.86	0.0015
MESMA	**0.92**	**0.84**	**0.99**	**0.75**	**0.0045**	**0.93**	**0.91**	**0.97**	**0.85**	**0.0022**	**0.95**	**0.94**	**0.97**	**0.89**	**0.0013**

Note 1: Bold values represent the most accurate estimation.
Note 2: All estimations are significantly different in the three study areas.

Table 5
Surface coal mining affected area (SCMAA), expressed in absolute and relative values.

Image	Spain		USA		Australia	
	km^2	% total	km^2	% total	km^2	% total
NDVI	360.28	20.15	150.73	10.28	205.82	10.42
MSAVI	197.25	11.03	46.06	3.14	63.51	3.22
SMA	43.63	2.44	173.47	11.83	198.97	10.08
MESMA	**27.38**	**1.53**	**83.91**	**5.72**	**163.90**	**8.30**
Ground Reference	29.36	1.64	78.68	5.36	158.59	8.03

Note: Bold values represent the most accurate estimation.

A relevant aspect of our study is the comparison of different methods to map SCMAA on three different forest ecosystems. The importance of our work is higher when considering the low number of studies relating remote sensing and mining activities compared to the high importance of coal mining in the world. Previously, most, studies have focused on a single region (Bernhardt & Palmer, 2011; Connor et al., 2004; Pond et al., 2008). We are unaware of any study that evaluates the effects of surface coal mining in Africa, where such economic activity has an important economic and spatial relevance. Our comparison among the results obtained in three continents (America, Europe, and Australia) determined that although local conditions can have an influence on the results (we observed small differences among the three study areas), it is possible to develop a globally applicable model using the proposed MESMA-based method.

5. Conclusions

SCM has an important economic, social and environmental impact at the global scale. SCM, particularly mountain top removal, causes

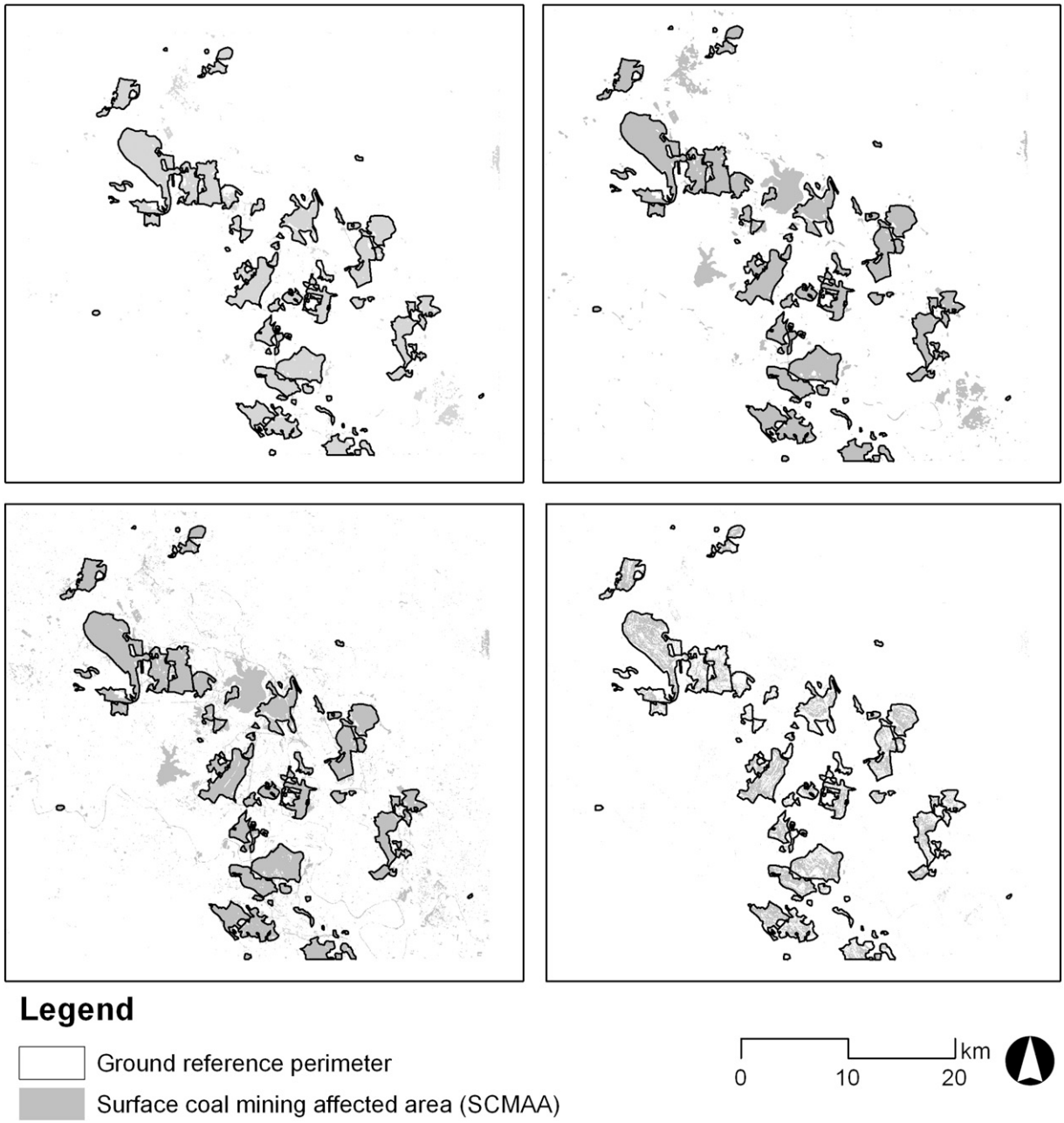

Fig. 7. Surface coal mining affected area (SCMAA) estimated in the Australian study area. Upper left: MESMA-based SCMAA estimation; upper right: SMA-based SCMAA estimation; down left: NDVI-based SCMAA estimation; down right: MSAVI-based SCMAA estimation.

disruption and degradation over wide regions of the world. The development of energy policies, environmental and social issues associated with the coal resources needs a reliable source of information to be contrasted. The study, for the first time evaluates the potential of remote sensing to accurately map SCMAA at a global scale.

We analyzed the potential of MESMA to accurately map SCMAA from Landsat data and to increase the accuracy obtained by conventional methods such as the classifying NDVI image. We have shown that MESMA can be successfully applied to Landsat data to accurately locate and quantify SCMAA. The building of a spectral library comprising both image endmembers and reference endmembers from AVIRIS image helped in the characterization of SCMAA. EAR, MASA and CoB lead to an optimal selection of endmembers finally used. We demonstrated that MESMA using these three endmembers: GV&NPV (biotic), SCM&SOIL (abiotic), and shade, out-performed simple SMA and spectral indices when SCMAA modeling is considered. In the three study areas, results showed a significant improvement in the accuracy of the SCMAA estimates when MESMA was used. We conclude that the presented MESMA-based approach has a high potential to map accurately SCMAA in different world forest ecosystems.

We showed that the remote sensing techniques used in this study are useful tools, capable of aiding in the process of monitoring forest cover changes caused by mining activities. As remote sensing technology advances, its potential role in monitoring surface mining and reclamation will be enhanced. This study provides a basis upon which future research can build and it is an open research line with a great potential for extracting information from multispectral satellite imagery.

Acknowledgements

This work was funded in part by Spanish Education Ministry grants (Salvador de Madariaga program) to the two first authors (codes PR2011-0555 and PR2011-0556, respectively) to support a research visit at VIPER Lab. (University of California, Santa Barbara). Equally, all the authors would like to thank the Ministry of Environment of the Castilla y León regional government for its collaboration in this work.

References

Adams, J. B., & Gillespie, A. R. (2006). Remote Sensing of Landscapes with Spectral Images. *A Physical Modeling Approach*. New York: Cambridge University Press (Ed. 362 pp.).

AEMET (2011). Climate services (database). Spanish Meteorological Agency. http://www.aemet.es/ (last accessed 15 December 2011).

Bedini, E., van der Meer, F., & van Ruitenbeek, F. (2009). Use of HyMap imaging spectrometer data to map mineralogy in the Rodalquilar caldera, southeast Spain. *International Journal of Remote Sensing*, *30*, 327–348.

Bernhardt, E., & Palmer, M. A. (2011). The environmental costs of mountaintop mining valley fill operations for aquatic ecosystems of the Central Appalachians. *Annals of the New York Academy of Sciences. The Year in Ecology and Conservation Biology*, *1223*(1), 39–57.

Boardman, J. W., & Kruse, F. A. (1994). Automated spectral analysis: A geologic example using AVIRIS data, north Grapevine Mountains, Nevada. *Proceedings of Tenth Thematic Conference on Geologic Remote Sensing*. Ann Arbor, MI: Environmental, Research Institute of Michigan p. I-407–I-418.

Boardman, J. W., Kruse, F. A., & Green, R. O. (1995). Mapping target signatures via partial unmixing of AVIRIS data, Summaries. *Fourth JPL Airborne Geoscience Workshop, JPL Publication*, *1*. (pp. 23–26).

Chander, G., & Markham, B. (2003). Revised Landsat-5 TM radiometric calibration procedures and postcalibration dynamic ranges. *IEEE Transactions on Geoscience and Remote Sensing*, *41*, 2674–2677.

Charou, E., Stefouli, M., Dimitrakopoulos, D., Vasiliou, E., & Mavrantza, O. D. (2010). Using remote sensing to assess impact of mining activities on land and water resources. *Mine Water Environment*, *29*, 45–52.

Chavez, P. S., Jr. (1989). Radiometric calibration of Landsat Thematic Mapper multispectral images. *Photogrammetric Engineering and Remote Sensing*, *55*, 1285–1294.

Chavez, P. S., Jr. (1996). Image-based atmospheric corrections — Revisited and improved. *Photogrammetric Engineering and Remote Sensing*, *62*, 1025–1036.

Congalton, R. G., & Green, K. (2009). *Assessing the accuracy of remotely sensed data. Principles and practices* (2 edition). Boca Ratón: CRC Press. Taylor & Francis.

Connor, L., Albrecht, G., Higginbotham, N., Freeman, S., & Smith, W. (2004). Environmental change and human health in upper hunter communities of New South Wales, Australia. *EcoHealth*, *1*, 47–58.

Dennison, P. E., Halligan, K. Q., & Roberts, D. A. (2004). A comparison of error metrics and constraints for multiple endmember spectral mixture analysis and spectral angle mapper. *Remote Sensing of Environment*, *93*, 359–367.

Dennison, P. E., & Roberts, D. A. (2003a). The effects of vegetation phenology on endmember selection and species mapping in Southern California Chaparral. *Remote Sensing of Environment*, *87*, 295–309.

Dennison, P. E., & Roberts, D. A. (2003b). Endmember selection for multiple endmember spectral mixture analysis using endmember average RMSE. *Remote Sensing of Environment*, *87*, 123–135.

Dennison, P. E., Roberts, D. A., & Peterson, S. H. (2007). Spectral shape-based temporal compositing algorithms for MODIS surface reflectance data. *Remote Sensing of Environment*, *109*, 510–522.

Department for Energy Development and Independence (DEDI) (2010). *Kentucky Energy Profile 2010*.

Ellis, R. J., & Scott, P. W. (2004). Evaluation of hyperspectral remote sensing as a means of environmental monitoring in the St. Austell China clay (kaolin) region, Cornwall, UK. *Remote Sensing of Environment*, *93*, 118–130.

Environment for Visualizing Images (ENVI) Software v.4.7 (2009). ITT Visual Information Solution. www.ittivis.com.

Erener, A. (2011). Remote sensing of vegetation health for reclaimed areas of Seyitömer open cast coal mine. *International Journal of Coal Geology*, *86*, 20–26.

Fernández-Manso, O., Fernández-Manso, A., Quintano, C., & Álvarez, F. (2005). Mapping forest cover changes caused by mining activities using spectral mixture analysis and object oriented classification. *ForestSat 2005 -Scientific workshop in operational tools in forestry using remote sensing techniques. May 31 - June 3, 2005, Borås -Sweden.* In Hákan Olsson (Ed.), *Proceedings of ForestSat 2005 — Scientific workshop in operational tools in forestry using remote sensing techniques* ISSN 1100–0295. p. 8c: 77–81 p. 8c: 77-81.

García-Criado, F., Tome, A., Vega, F. J., & Antolin, C. (1999). Performance of some diversity and biotic indices in rivers affected by coal mining in northwestern Spain. *Hydrobiologia*, *394*, 209–217.

Haruna, D. M., & Salomon, N. J. (2011). An assessment of mining activities impact on vegetation in Bukuru Jos Plateau State Nigeria using Normalized Differential Vegetation Index (NDVI). *Journal of Sustainable Development*, *4*, 150–159.

Herold, M., Roberts, D. A., Gardner, M. E., & Dennison, P. E. (2004). Spectrometry for urban area remote sensing. Development and analysis of a spectral library from 350 to 2400 nm. *Remote Sensing of Environment*, *91*, 304–319.

International Energy Agency (IEA) (2011). *CO_2 emissions from fuel combustion*. Paris: Highlights IEA Publications.

Jensen, J. R. (1996). *Introductory digital image processing a remote sensing perspective*. Upper Saddle River, New Jersey: Prentice Hall 316 pp.

Kaufman, Y. J. (1989). The atmospheric effect on remote sensing and its corrections. In G. Asrar (Ed.), *Theory and applications of optical remote sensing* (pp. 336–428). New York, NY: Wiley-Interscience.

Kennedy, A. J., Cherry, D. S., & Currie, R. J. (2003). Field and laboratory assessment of a coal processing effluent in the Leading Creek watershed, Meigs County, Ohio. *Archives of Environmental Contamination and Toxicology*, *44*, 324–331.

Latifovic, R., Fytas, K., Chen, J., & Paraszczak, J. (2005). Assessing land cover change resulting from large surface mining development. *International Journal of Applied Earth Observation and Geoinformation*, *7*, 29–48.

Lévesque, J., & Staenz, K. (2008). A method for monitoring mine tailings re-vegetation using hyperspectral remote sensing. *Proceedings of 2004 IEEE International Geoscience and Remote Sensing Symposium (IGARSS 2004), 20–24 September 2004, Anchorage, AK* (pp. 575–587).

Li, L., Ustin, S. L., & Lay, M. (2005). Application of multiple endmember spectral mixture analysis (MESMA) to AVIRIS imagery for coastal salt marsh mapping: A case study in China Camp, CA, USA. *International Journal of Remote Sensing*, *26*, 5193–5207.

Liu, A., & Wang, J. (2005). Monitoring desertification in arid and semi-arid areas of China with NOAA-AVHRR and MODIS data. *Proceedings of 2005 IEEE Geoscience and Remote Sensing Symposium (IGARSS 2005)*.

Lu, D., & Weng, Q. (2004). Spectral mixture analysis of the urban landscape in Indianapolis with Landsat ETM + imagery. *Photogrammetric Engineering and Remote Sensing*, *70*, 1053–1062.

Mansor, B., Cracknell, A. P., Shilin, B. V., & Gornyi, V. I. (1994). Monitoring of underground coal fires using thermal infrared data. *International Journal of Remote Sensing*, *15*, 1675–1685.

Mars, J. C., & Crowley, J. K. (2003). Mapping mine wastes and analyzing areas affected by selenium-rich water runoff in southeast Idaho using AVIRIS imagery and digital elevation data. *Remote Sensing of Environment*, *84*, 422–436.

Martha, T. R., Guha, A., Kumar, K. V., Kamaraju, M. V. V., & Raju, E. V. R. (2010). Recent coal-fire and land-use status of Jharia Coalfield, India from satellite data. *International Journal of Remote Sensing*, *31*, 3243–3262.

Minerals Council of Australia (2010). *Vision 2020 Project: The Australian Minerals Industry's Infrastructure, Path to Prosperity. New South Wales.*

Nuray, D., Emila, M. K., & Duzguna, H. S. (2011). Surface coal mine area monitoring using multi-temporal high-resolution satellite imagery. *International Journal of Coal Geology*, *86*, 3–11.

Palmer, M. A., Bernhardt, E. S., Schlesinger, W. H., Eshleman, K. N., Foufoula-Georgiou, E., Hendryx, M. S., et al. (2010). Mountaintop mining consequences. *Science and Regulation*, *327*, 148–149.

Parks, N. F., Peterson, G. W., & Baumer, G. M. (1987). High resolution remote sensing of spatially and spectrally complex coal surface mines of Central Pennsylvania: A comparison between SPOT, MSS and Landsat-TM. *Photogrammetric Engineering and Remote Sensing*, *53*, 415–420.

Pond, G. J., Passmore, M. E., Borsuk, F. A., Reynolds, L., & Rose, C. J. (2008). Downstream effects of mountaintop coal mining: Comparing biological conditions using family-

and genus-level macroinvertebrate bioassessment tools. *Journal of the North American Benthological Society*, *27*, 717–737.
Prakash, A., & Gupta, R. P. (1998). Land-use mapping and change detection in a coal mining area: A case study in the Jharia Coalfield, India. *International Journal of Remote Sensing*, *19*, 391–410.
Qi, J., Chehbouni, A., Huete, A. R., & Kerr, Y. H. (1994a). Modified Soil Adjusted Vegetation Index (MSAVI). *Remote Sensing of Environment*, *48*, 119–126.
Qi, J., Kerr, Y., & Chehbouni, A. (1994b). External factor consideration in vegetation index development. *Proceedings of Physical Measurements and Signatures in Remote Sensing, ISPRS*, 723–730.
Quintano, C., Fernández-Manso, A., Fernández-Manso, O., & Shimabukuro, Y. (2006). Mapping burned areas in Mediterranean countries using Spectral Mixture Analysis from a unitemporal perspective. *International Journal of Remote Sensing*, *27*, 645–662.
Rashed, T., Weeks, J. R., Roberts, D., Rogan, J., & Powell, R. (2003). Measuring the physical composition of urban morphology using multiple endmember spectral mixture models. *Photogrammetric Engineering and Remote Sensing*, *69*, 1011–1020.
Rathore, C. S., & Wright, R. (1993). Monitoring environmental impacts of surface coalmining. *International Journal of Remote Sensing*, *14*, 1021–1042.
Richter, N., Staenz, K., & Kaufmann, H. (2008). Spectral unmixing of airborne hyperspectral data for baseline mapping of mine tailings areas. *International Journal of Remote Sensing*, *29*, 3937–3956.
Roberts, D. A., Dennison, P. E., Gardner, M., Hetzel, Y., Ustin, S. L., & Lee, C. (2003). Evaluation of the potential of hyperion for fire danger assessment by comparison to the airborne visible/infrared imaging spectrometer. *IEEE Transactions on Geoscience and Remote Sensing*, *41*, 1297–1310.
Roberts, D. A., Gardner, M., Church, R., Ustin, S. L., Scheer, G., & Green, R. O. (1998). Mapping Chaparral in the Santa Monica Mountains using multiple endmember spectral mixture models. *Remote Sensing of Environment*, *65*, 267–279.
Roberts, D. A., Halligan, K., & Dennison, P. (2007). *VIPER Tools User Manual. V1.5.*
Roberts, D. A., Quattrochi, D. A., Hulley, G. C., Hook, S. J., & Green, R. O. (2012). Synergies between VSWIR and TIR data for the urban environment: An evaluation of the potential for the Hyperspectral Infrared Imager (HyspIRI) Decadal Survey mission. *Remote Sensing of Environment*, *117*, 83–101.
Rouse, J. W., Haas, R. H., Schell, J. A., & Deering, D. W. (1973). Monitoring vegetation systems in the great plains with ERTS. *Third ERTS Symposium, NASA SP-351, NASA, Washington, DC*, *Vol. 1*. (pp. 309–317).
Schmidt, H., & Glaesser, C. (1998). Multitemporal analysis of satellite data and their use in the monitoring of the environmental impacts of open cast lignite mining areas in Eastern Germany. *International Journal of Remote Sensing*, *12*, 2245–2260.
Schroeter, L. E. (2011). Analyses and monitoring of lignite mining lakes in Eastern Germany with spectral signatures of Landsat TM satellite data. *International Journal of Coal Geology*, *86*, 27–39.
Shang, J., Morris, B., Howarth, P., Lévesque, J., Staenz, K., & Neville, B. (2009). Mapping mine tailing surface mineralogy using hyperspectral remote sensing. *Canadian Journal of Remote Sensing/Journal canadien de Télédétection*, *3*, S126–S141.
Shank, M. (2008). Using remote sensing to map vegetation density on a reclaimed surface mine. *Proceedings of "Incorporating Geospatial Technologies into SMCRA Business Processes", March 25–27, 2008, Atlanta, GA*.
Slonecker, E. T., & Benger, M. J. (2002). Remote sensing and mountaintop mining. *Remote Sensing Reviews*, *20*, 293–322.
Song, C., Woodcock, C. E., Seto, K. C., Lenney, M. P., & Macomber, S. A. (2001). Classification and Change Detection Using Landsat TM Data: When and How to Correct Atmospheric Effects? *Remote Sensing of Environment*, *75*, 230–244.
Spanish Ministry of Industry, Tourism and Business (2009). *Methane to Markets.* Partnership Coal Subcommittee — CMM Global Overview, EURACOAL.
Straker, J., Blazecka, M., Sharman, K., Woelk, S., Boorman, S., & Kuschminder, J. (2004). Use of remote sensing in reclamation assessment at Teck Cominco's Bullmoose Mine Site. B.C. *Mine Reclamation Symposium 2004*.
Teillet, P. M., Guindon, B., & Goodenough, D. G. (1982). On the slope-aspect correction of multispectral scanner data. *Canadian Journal of Remote Sensing/Journal canadien de Télédétection*, *8*, 84–106.
Thomas, V., Gellie, N., & Harrison, T. (2000). *Forest ecosystem classification and mapping for the Southern CRA Region. Volume 1.* Sydney: NSW National Parks and Wildlife Service 46 pp.
Tompkins, S., Mustard, J. F., Pieters, C. M., & Forsyth, D. W. (1997). Optimization of endmembers for spectral mixture analysis. *Remote Sensing of Environment*, *59*, 472–489.
Toren, T., & Ünal, E. (2001). Assessment of open pit coal mining impacts using remote sensing: A case study from Turkey. *17th International Mining Congress and Exhibition of Turkey- IMCET2001, 2001*. Ankara, Turkey: General Directorate of Turkish Coal Enterprises975-395-417-4.
Townsend, P. A., Helmers, D. P., Kingdon, C. C., McNeil, B. E., de Beurs, K. M., & Eshleman, K. N. (2009). Changes in the extent of surface mining and reclamation in the Central Appalachians detected using a 1976–2006 Landsat time series. *Remote Sensing of Environment*, *113*, 62–72.
United States Energy Information Administration (EIA) (2011). *Annual Energy Review 2010.* Washington, DC 20585: Office of Energy Statistics, U.S. Department of Energy.
Voigt, S., Tetzlaff, A., Zhang, J., Künzer, C., Zhukov, B., Strunz, G., et al. (2004). Integrating satellite remote sensing techniques for detection and analysis of uncontrolled coal seam fires in North China. *International Journal of Coal Geology*, *59*, 121–136.
Wen-bo, W., Jing, Y., & Ting-Jun, K. (2008). Study on land use changes of the coal mining area based on TM image. *Journal of Coal Science and Engineering*, *14*, 287–290.
World Coal Association (2005). *The coal resource — A comprehensive overview of coal.* World Coal Association.
Wright, P., & Stow, R. (1999). Detecting mining subsidence from space. *International Journal of Remote Sensing*, *20*, 1183–1188.
Wu, C. (2004). Normalized spectral mixture analysis for monitoring urban composition using ETM + imagery. *Remote Sensing of Environment*, *93*, 480–492.
Wuebbles, D. J., & Hayhoe, K. (2002). Atmospheric methane and global change. *Earth-Science Reviews*, *57*, 177–210.